Journal of
Materials Chemistry C

PAPER

View Article Online
View Journal

Cite this: DOI: 10.1039/c5tc00409h

Novel 1,8-naphthalimide derivatives for standard-red organic light-emitting device applications†

Shuai Luo,‡[a] Jie Lin,‡[b] Jie Zhou,[a] Yi Wang,[a] Xingyuan Liu,*[b] Yan Huang,[a] Zhiyun Lu*[a] and Changwei Hu*[a]

Received 11th February 2015,
Accepted 11th April 2015

DOI: 10.1039/c5tc00409h

www.rsc.org/MaterialsC

Three red-emissive D–π–A-structured fluorophores with an aromatic amine as the donor, ethene-1,2-diyl as the π-bridge, and 1,8-naphthalimide as the acceptor subunit, namely, (*E*)-6-(4-(dimethylamino)styryl)-2-hexyl-1*H*-benzo[*de*]isoquinoline-1,3(2*H*)-dione (**Nap1**), (*E*)-2-(2,6-di(isopropyl)phenyl)-6-(4-(dimethylamino)-styryl)-1*H*-benzo[*de*]isoquinoline-1,3(2*H*)-dione (**Nap2**) and (*E*)-2-(2,6-di(isopropyl)phenyl)-6-(2-(1,1,7,7-tetramethyl-2,3,6,7-tetrahydro-1*H*,5*H*-pyrido[3,2,1-*ij*]quinolin-9-yl)vinyl)-1*H*-benzo[*de*]isoquinoline-1,3(2*H*)-dione (**Nap3**), were designed and synthesized. In-depth investigations on the correlations between their molecular structures and photophysical characteristics revealed that the presence of an electron-rich 4-dimethylaminophenyl donor moiety in compound **Nap1** could endow it with a red emission (*e.g.*, $\lambda_{PL\,max}$ = 641 nm in the host–guest blend film with a 14 wt% guest composition); moreover, the replacement of the *n*-hexyl group of **Nap1** bonding to the imide nitrogen atom for a more bulky 2,6-di(isopropyl)phenyl one would result in compound **Nap2** with more alleviated concentration quenching. Alteration of the 4-(dimethylamino)phenyl donor subunit of **Nap2** into a more electron-donating 1,1,7,7-tetramethyljulolidin-9-yl substituent would render compound **Nap3** with more improved chromaticity (*e.g.*, $\lambda_{PL\,max}$ = 663 nm in a 14 wt% guest-doped film). Consequently, **Nap3** could not only emit standard-red fluorescence with satisfactory chromaticity, but it also showed suppressed intermolecular interactions. Using **Nap3** as the dopant, a heavily doped standard-red organic light-emitting diode (OLED) with the device configuration of ITO/MoO_3 (1 nm)/TcTa (40 nm)/**CzPhONI**:**Nap3** (14 wt%) (20 nm)/TPBI (45 nm)/LiF (1 nm)/Al (80 nm) was fabricated, and the Commission Internationale de L'Eclairage coordinates, maximum external quantum efficiency and maximum current efficiency of this OLED were (0.67,0.32), 1.8% and 0.7 cd A^{-1}, respectively. All these preliminary results indicated that 1,8-naphthalimide derivatives could act as quite promising standard-red light-emitting materials for OLED applications.

1. Introduction

Owing to their merits like solid-state self-emission, wide viewing angle, facile color tunability and processability, organic light-emitting devices (OLEDs) have been considered as quite competitive candidates for flat-panel display applications.[1] In comparison with phosphorescent OLEDs, fluorescent ones are more suitable with respect to display applications due to their faster response as well as lower efficiency roll-off.[2] For full-color display applications, it is necessary to develop red, green, and blue fluorescent OLEDs with high efficiency and appropriate chromaticity, yet compared with that of blue[3a] and green[3b] devices, the performance of red fluorescent OLEDs with good chromaticity is unsatisfactory. For example, although the current efficiency (CE) of red OLEDs with Commission Internationale de L'Eclairage (CIE) coordinates of (0.63,0.37) could reach 11.5 cd A^{-1},[4] their chromaticity is far from standard-red whose CIE coordinates should be close to (0.67,0.33) according to the stipulation from the National Television Standards Committee. As far as standard-red OLEDs are concerned, although according to a technical report from Idemitsu Kosan Co., high performance devices with CE of 11.0 cd A^{-1} could be achieved,[5] no detailed information about the molecular structures of the emitting materials and the device structures could be found.

[a] *Key Laboratory of Green Chemistry and Technology of Ministry of Education, College of Chemistry, Sichuan University, Chengdu, 610064, P. R. China. E-mail: luzhiyun@scu.edu.cn, changweihu@scu.edu.cn*
[b] *State Key Laboratory of Luminescence and Applications, Changchun Institute of Optics, Fine Mechanics and Physics, Chinese Academy of Sciences, Changchun 130033, P. R. China. E-mail: liuxy@ciomp.ac.cn*

† Electronic supplementary information (ESI) available: Lippert–Mataga plots of **Nap1–3**, cyclic voltammograms of **Nap1–3**, EL spectra of devices **I–III**, current efficiency–current density characteristics of devices **I–III**, ^{1}H NMR, ^{13}C NMR, FT-IR, and HRMS spectra of **Nap1–3**. See DOI: 10.1039/c5tc00409h

‡ These authors contributed equally.

In scientific literature reports, the performance of standard-red OLEDs is rather poor with the maximum CE values lower than 3.0 cd A^{-1} and external quantum efficiencies (EQEs) less than 4.0%.[6] In addition, due to the notorious concentration quenching of the guest fluorophores, the best standard-red OLED bearing guest–host doping structure (CE_{max}: 1.6 cd A^{-1}) has just a low doping-level of 2 wt%;[6d] hence the manufacturing process should be precisely controlled to acquire good device reproducibility.[7] Consequently, it is highly desired to exploit novel high performance standard-red fluorophores with suppressed concentration quenching,[6c,8] so that OLEDs with relatively high doping-levels or even self-hosted device structure could be achieved.

In general, red electrofluorescent materials could be classified into two main categories, namely, compounds bearing polycyclic aromatic hydrocarbon (PAHs) structures and compounds showing intramolecular charge-transfer (ICT) characteristic with D–π–A molecular structures (where D denotes electron-donor and A denotes electron-acceptor).[8–10] To acquire standard-red fluorescence, PAHs compounds should possess relatively large conjugation systems, *e.g.*, polyacenes[11a] and porphyrins.[11b,c] However, to prepare these compounds, delicate synthetic and purifying procedures have to be involved.[12] In addition, serious concentration quenching is often observed in these PAHs due to their intense intermolecular interactions.[10] By contrast, ICT-featured red fluorophores bearing D–π–A molecular skeletons have attracted much attention due to their more facile molecular tailoring.[13] Currently, the reported red electrofluorescent ICT-compounds could be assorted, according to their acceptor constructive units, as maleimide derivatives,[14] benzothiadiazole derivatives,[15] fumaronitrile derivatives,[6f,16] and 4-dicyanomethylene-4*H*-pyran derivatives,[17] *etc*. However, despite the fact that 1,8-naphthalimide is a widely used acceptor subunit for constructing high performance green[18] and yellow[19] ICT-featured electroluminescent (EL) materials, quite limited success has been achieved in terms of high performance orange and red ones. In 2003, using 1,8-naphthalimide and quinoxaline as the acceptor segments, Lee *et al.*[20] reported an naphthalimide luminogen, but the OLED based on it could only emit orange-red EL with $\lambda_{EL\,max}$ of 608 nm. Subsequently, Tian *et al.*[21] reported that D–A fluorophores with 1,8-naphthalimide as the acceptor subunit could act as red EL materials, yet both the chromaticity and the performance of the OLED were unsatisfactory ($\lambda_{EL\,max}$ = 620 nm, L_{max} (maximum brightness) is 15 cd m^{-2}). Although in 2005, Cheng *et al.*[22] fabricated red OLEDs with CIE coordinates of (0.63,0.36) using 1,8-naphthalic anhydride derivatives as light-emitting materials, the CE_{max} of these devices was as low as 0.6 cd A^{-1}. Nevertheless, our recent study has revealed that a 1,8-naphthalimide derivative could act as a high performance orange EL guest material, and the corresponding OLED shows a CE_{max} of 7.2 cd A^{-1}, EQE_{max} of 3.6%, and L_{max} of 16 800 cd m^{-2}.[23] Despite the fact that the CIE coordinates of this device was just (0.56,0.44), its high performance has triggered our speculation that through rational molecular design, 1,8-naphthalimide derivatives may also act as quite promising standard-red EL materials.

Recently, it has been reported that the D–π–A-structured 1,8-naphthalimide derivative **NIM** (structure shown in Fig. 1) could emit intense orange fluorescence in the solid state ($\lambda_{PL\,max}$ = 597 nm).[24] To construct fluorophores with more red-shifted photoluminescence (PL) emission bands than that of **NIM**, herein, we altered the 4-(diphenylamino)phenyl (DPAP) donor segment of **NIM** to be a more electron-rich 4-(dimethylamino)-phenyl (DMAP) or 1,1,7,7-tetramethyljulolidin-9-yl (TMJ) donor segment, and constructed three objective compounds (**Nap1–3**, structures shown in Fig. 1). Moreover, to alleviate the intermolecular interactions, a bulky 2,6-di(isopropyl)phenyl substituent was bonded to the imide nitrogen atom of **Nap2** and **Nap3**. As expected, **Nap1–3** all could emit standard-red fluorescence in the thin solid film state, and **Nap2** and **Nap3** showed more suppressed concentration quenching than **Nap1**. Using **Nap3** as the guest dopant, a high performance standard-red OLED with a relatively heavy doping-level of 14 wt% was achieved. The device had CIE coordinates of (0.67,0.32), EQE_{max} of 1.8%, and a CE_{max} of 0.7 cd A^{-1}, indicating that 1,8-naphthalimide derivatives should be promising candidates as high performance standard-red EL materials.

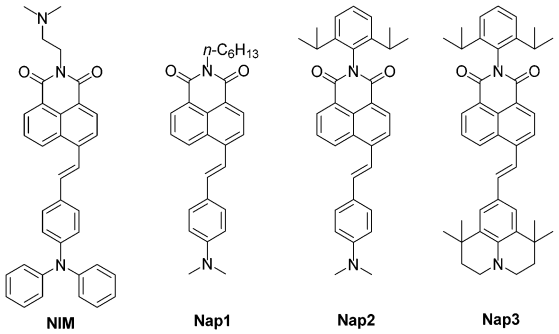

Fig. 1 Molecular structures of **NIM**, **Nap1**, **Nap2** and **Nap3**.

2. Experimental section

2.1 General information

All the reagents involved in the synthetic procedures were commercially available and used without purification unless otherwise stated. Cyclohexane (CHX), tetrachloromethane, toluene (Tol), chloroform, tetrahydrofuran (THF), dichloromethane (DCM), acetone, *N,N*-dimethyl formamide (DMF) were of analytical grade and were distilled freshly prior to use. ^{1}H NMR and ^{13}C NMR spectra were obtained on a BRUKER AVANCE AV II-400 MHz spectrometer in DMSO-d_6 or $CDCl_3$ using TMS as the internal standard. High resolution MS spectra were obtained on a Shimadzu LCMS-IT-TOF spectrometer. FT-IR spectra were obtained on a Perkin-Elmer 2000 infrared spectrometer with KBr pellets under an ambient atmosphere. UV-Vis absorption spectra were obtained on a Perkin-Elmer Lambda 950 scanning spectrophotometer. PL spectra were obtained on a Perkin-Elmer LS55 fluorescence spectrophotometer at 298 K. The absolute PL quantum yields (QYs) of both solution and film samples were determined on a FluoroMax-4 spectrofluorometer (Horiba Jobin Yvon) equipped with an integrating sphere and a digital photometer. Both the fluorimeters have been corrected for the wavelength

dependence of the sensitivity of the detectors and throughput of the monochromators. The **Nap–CzPhONI** composite as well as the **Nap** neat thin film samples were spin-coated from their corresponding chloroform solutions with a concentration of 10 mg mL^{-1} at a speed of 1500 rpm on quartz substrates for 40 s. Cyclic voltammetry measurements were performed in anhydrous acetonitrile (5×10^{-4} mol L^{-1}) solutions of **Nap1–3** using 0.10 mol L^{-1} Bu_4NClO_4 as the supporting electrolyte under a N_2 atmosphere on a LK 2010A electrochemical work station at room temperature, and the three-electrode cell comprised a Pt working electrode, a Pt wire counter electrode, and a $Ag/AgNO_3$ (0.1 M in acetonitrile) reference electrode. A ferrocene/ferrocenium redox couple was employed as the external standard.

2.2 OLED fabrication and measurements

Indium-tin oxide (ITO) coated glass substrates were cleaned by ultrasonic mixing successively in alcohol, acetone, methanol, and deionized water, followed by UV-ozone oxygen plasma treatment for 2 min before use. Organic functional layers were thermo-evaporated in vacuum (3×10^{-4} Pa) with a deposition rate of 0.1 nm s^{-1}. After deposition of the organic layers, the LiF–Al cathode was prepared first by thermal deposition of a LiF thin film (1 nm) followed by the deposition of an Al layer (80 nm). The active area of the OLEDs was 1×1 mm^2. The thicknesses of the organic layers and the cathode were controlled using a quartz crystal thickness monitor. The luminance–voltage–current density (*L–V–J*) characteristics of the OLEDs were measured with a Keithley 2611 Source Meter and a PR705 Spectra Colorimeter, which can also record EL spectra and CIE coordinates accurately. All the measurements on the devices were carried out in an ambient atmosphere without further encapsulation.

2.3 Synthesis

The synthetic routes to **Nap1–3** are outlined in Scheme 1. Intermediates **2**,[25] **3**,[26] **5**,[27] **6**[28] were synthesised according to literature reports.

1,1,7,7-Tetramethyl-9-vinyl-2,3,6,7-tetrahydro-1*H*,5*H*-pyrido-[3,2,1-*ij*]quinolone (4). *n*-Butyl lithium (1.0 mL of 2.5 mol L^{-1} in *n*-hexane solution) was added dropwise to a suspension of PPh_3CH_3Br (0.90 g, 2.3 mmol) in anhydrous degassed THF (10.0 mL). The yellow solution was allowed to stir for 30 min, then a solution of **3** (0.4 g, 1.6 mmol) in 5.0 mL anhydrous degassed THF was added. After being stirred for 20 min, the yellow suspension was poured into saturated aqueous ammonium chloride, and then extracted by petroleum ether (4×15 mL). The organic layer was dried over anhydrous Na_2SO_4, and concentrated in vacuum. The resulting crude product was purified by silica gel column chromatography (eluent: petroleum ether/ethyl acetate = 20/1, v/v) to give **4** as a yellowish liquid (0.3 g, 50%). δ_H (400 MHz; $CDCl_3$; Me_4Si) 7.07 (2H, s, ArH), 6.62 (1H, dd, J_1 = 17.2 Hz, J_2 = 10.8 Hz, ═CH), 5.51 (1H, dd, J_1 = 17.6 Hz, J_2 = 1.6 Hz, ═CH), 4.99 (d, J_1 = 10.0 Hz, J_2 = 1.6 Hz, 1H, ═CH), 3.18 (t, J = 6.0 Hz, 6H, $-NCH_2$), 1.45 (t, J = 6.0 Hz, 1H, Ar–CH_2), 1.30 (s, 12H, $-CH_3$).

(*E*)-6-(4-(Dimethylamino)styryl)-2-hexyl-1*H*-benzo[*de*] isoquinoline-1,3(2*H*)-dione (Nap1). A Schlenk flask was charged with a mixture of **2** (0.13 g, 0.9 mmol), **5** (0.30 g, 0.9 mmol), $Pd(OAc)_2$ (3.5 mg, 0.02 mmol), P(*o*-tolyl)$_3$ (8.3 mg, 0.03 mmol), triethylamine (6.0 mL) and *N*,*N*-dimethylformamide (DMF) (7.0 mL). The reaction mixture was heated at 90 °C for 24 h under argon. After being cooled to room temperature, the mixture was poured into water (100 mL), extracted by dichloromethane (4×20 mL) and then organic phase was combined and washed with brine and then dried over anhydrous Na_2SO_4. After the solvent was removed under vacuum, the crude product was purified by column chromatography over a silica gel (eluent: petroleum ether/dichloromethane = 15/1, v/v), followed by recrystallization from a mixture of cyclohexane and dichloromethane to afford pure **Nap1** as a red solid (0.1 g, 30%). δ_H (400 MHz; DMSO-d_6; Me_4Si) 9.00 (1H, d, J = 9.2 Hz, ArH), 8.53 (1H, d, J = 7.2 Hz, ArH), 8.45 (1H, d, J = 8.0 Hz, ArH), 8.21 (1H, d, J = 8.4 Hz, ArH), 7.96 (1H, d, J = 16.0 Hz, ═CH), 7.89 (1H, t, J_1 = 7.6 Hz, J_2 = 8.0 Hz, ArH), 7.71 (2H, d, J = 8.4 Hz, ArH), 7.55 (1H, d, J = 16.0 Hz, ═CH), 6.89 (2H, d, J = 8.4 Hz, ArH), 4.05 (2H, t, J = 7.2 Hz, $-NCH_2$), 3.00 (6H, s, $-NMe_2$), 1.64 (m, 2H, $-CH_2$, $-CH_3$), 1.31 (m, 6H, $-CH_2$), 0.87 (m, 3H, $-CH_3$). δ_C (100 MHz; $CDCl_3$; Me_4Si) 164.4, 164.2, 150.9, 142.4, 135.6, 131.2, 131.0, 130.1, 129.4, 128.9, 128.5, 126.3, 124.8, 123.1, 122.9, 118.4, 112.2, 40.5, 40.3, 31.6, 28.1, 26.8, 22.6, 14.1. FT-IR ν_{max}/cm^{-1} 1655 (C═O), 1358 (C–N). HRMS $(ESI)^+$ *m*/*z*: calcd for $[M + H]^+$: $C_{28}H_{31}N_2O_2^+$, 427.2380; found, 427.2365.

(*E*)-2-(2,6-Di(isopropyl)phenyl)-6-(4-(dimethylamino)styryl)-1*H*-benzo[*de*]isoquinoline-1,3(2*H*)-dione (Nap2). Compound **Nap2** was prepared as a red solid with a yield of 50% using a similar procedure for the synthesis of **Nap1**, but with **5** rather than **6** as the reactant. δ_H (400 MHz; DMSO-d_6; Me_4Si) 9.11 (1H, d, J = 8.8 Hz, ArH), 8.59 (1H, d, J = 6.8 Hz, ArH), 8.50 (1H, d, J = 8.0 Hz, ArH), 8.25 (1H, d, J = 8.0 Hz, ArH), 8.01 (1H, d, J = 16.0 Hz, ═CH), 7.93 (1H, t, J_1 = 6.4 Hz, J_2 = 8.0 Hz, ArH), 7.73 (2H, d, J = 8.8 Hz, ArH), 7.60 (1H, d, J = 15.6 Hz, ═CH), 7.45 (1H, t, J = 7.6 Hz, ArH), 7.33 (2H, d, J = 7.6 Hz, ArH), 6.78 (2H, d, J = 8.8 Hz, ArH), 3.00 (6H, s, $-NMe_2$), 2.66 (2H, m, Ar–CH) 1.05 (12H, d, J = 6.8 Hz, $-CH_3$). δ_C (100 MHz; $CDCl_3$; Me_4Si) 164.4, 164.2, 145.7, 142.8, 135.9, 131.7, 131.6, 131.1, 130.4, 129.6, 129.6, 129.4, 128.6, 126.4, 124.0, 123.1, 123.0, 120.4, 118.4, 112.4, 40.4, 29.1, 24.0, 8.1. FT-IR ν_{max}/cm^{-1} 1661 (C═O), 1352 (C–N). HRMS $(ESI)^+$ *m*/*z*: calcd for $[M + H]^+$: $C_{34}H_{35}N_2O_2^+$, 503.2693; found, 503.2676.

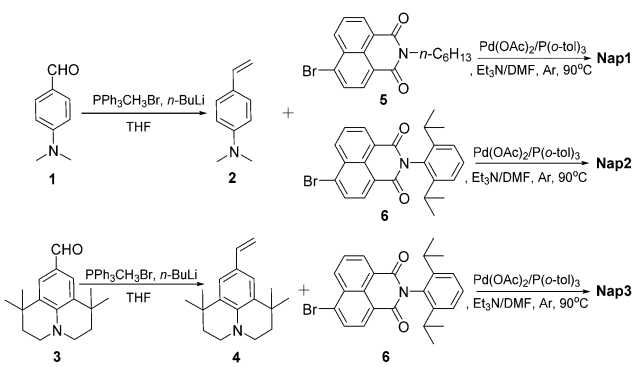

Scheme 1 Synthetic routes to the objective compounds.

(*E*)-2-(2,6-Di(isopropyl)phenyl)-6-(2-(1,1,7,7-tetramethyl-2,3,6,7-tetrahydro-1*H*,5*H*-pyrido[3,2,1-*ij*]quinolin-9-yl)vinyl)-1*H*-benzo[*de*]-isoquinoline-1,3(2*H*)-dione (Nap3). Compound **Nap3** was prepared as a dark red solid with a yield of 24% using a similar procedure as the synthesis of **Nap1**, but with **4** and **6** rather than **2** and **5** as the reactants. The crude product was purified by column chromatography over a silica gel (eluent: petroleum ether/dichloromethane = 15/1, v/v), followed by recrystallization from a mixture of *n*-hexane and dichloromethane three times. δ_H (400 MHz; DMSO-d_6; Me_4Si) 9.16 (1H, d, J = 8.4 Hz, ArH), 8.60 (1H, d, J = 7.2 Hz, ArH), 8.49 (1H, d, J = 8.0 Hz, ArH), 8.25 (1H, d, J = 8.0 Hz, ArH), 7.95 (2H, m, ArH, =CH), 7.57 (1H, d, J = 16.0 Hz, =CH), 7.52 (2H, s, ArH), 7.45 (1H, t, J_1 = 7.6 Hz, ArH), 7.34 (2H, d, J = 7.6 Hz, ArH), 3.23 (4H, t, J_1 = 6.4 Hz, J_2 = 6.0 Hz, $-NCH_2$), 2.67 (2H, m, Ar–CH), 1.73 (4H, t, J_1 = 5.6 Hz, J_2 = 6.0 Hz, $Ar-CH_2$), 1.32 (12H, s, $-CH_3$), 1.06 (12H, d, J = 4.0 Hz, $-CH_3$). δ_C (100 MHz; $CDCl_3$; Me_4Si) 164.5, 164.2, 145.7, 143.2, 137.0, 131.8, 131.6, 131.1, 130.5, 129.6, 129.4, 126.3, 123.9, 123.3, 123.1, 122.8, 119.9, 117.0, 46.8, 36.4, 32.3, 30.8, 29.1, 24.0. FT-IR ν_{max}/cm^{-1} 1661 (C=O), 1576 (C–N). HRMS $(ESI)^+$ m/z: calcd for $[M + H]^+$: $C_{42}H_{47}N_2O_2^+$, 611.3632; found, 611.3618.

3. Results and discussion

3.1 Photophysical properties in dilute solutions

The UV-Vis absorption spectra of **Nap1–3** in dilute solutions of different polarities are illustrated in Fig. 2, and the corresponding data are summarized in Table 1. In a similar solvent, the absorption maximum ($\lambda_{abs\,max}$) of **Nap2** is slightly red-shifted (~7 nm) compared with that of **Nap1**, but the $\lambda_{abs\,max}$ of **Nap3** was considerably red-shifted (>30 nm) compared to those of **Nap1** and **Nap2**. Therefore, the replacement of the *n*-hexyl bonding to the imide nitrogen atom into a 2,6-di(isopropyl) phenyl group would just bring a little effect on the conjugation length of these compounds, but the presence of a TMJ rather than a DMAP donor subunit in **Nap3** would endow it with a much extended π-conjugation system. As expected, in every solvent, the absorption bands of all the three objective compounds were red-shifted compared to that of **NIM**,[24] confirming that the bandgaps of **Nap1–3** are narrower than that of **NIM**, which should be chiefly attributed to the more electron-donating capability of DMAP and TMJ groups than that of DPAP. With an increase in solvent polarity from cyclohexane (CHX) to dichloromethane (DCM), the absorption bands of **Nap1–3** showed 20–30 nm red-shifts, indicative of the ICT character of the three compounds in their ground states.[20,29]

Consistent with the absorption characteristics of **NIM** and **Nap1–3**, the PL emission maximum ($\lambda_{PL\,max}$) of **Nap3** was more bathochromically-shifted (~30 nm) than that of **Nap2** or **Nap1** in every solvent, the $\lambda_{PL\,max}$ of **Nap2** was just slightly (3–5 nm) red-shifted compared to **Nap1**, and the $\lambda_{PL\,max}$s of **Nap1–3** are significantly red-shifted compared to **NIM** (Fig. 3 and Table 1). In comparison with their absorption spectra, the fluorescent spectra of **Nap1–3** show more significant positive solvatochromism (*e.g.*, for **Nap3**: $\lambda_{PL\,max}$ = 553 nm in CHX; $\lambda_{PL\,max}$ = 622 nm in toluene; $\lambda_{PL\,max}$ = 680 nm in chloroform; $\lambda_{PL\,max}$ = 722 nm in DCM; and $\lambda_{PL\,max}$ = 750 nm in acetone), indicating a strong ICT character of the lowest singlet excited states of **Nap1–3**. This deduction was further confirmed by the Lippert–Mataga plots of **Nap1–3** (see Fig. S1, ESI†), since good linear correlations between the solvent polarity parameter and Stokes shifts could be achieved in all these **Nap** systems. It should be pointed out that in solvents with moderate polarity like chloroform and tetrahydrofuran (THF), **Nap1–3** could emit red fluorescence with high PL quantum yields (PLQY, Φ_{PL}). For example, in THF solution, both **Nap1** and **Nap2** showed $\lambda_{PL\,max}$ values >650 nm and Φ_{PL} values >0.5, and the chloroform solution of **Nap3** displayed a $\lambda_{PL\,max}$ of 680 nm and a Φ_{PL} of 0.45. With further increased solvent polarity to acetone, the PL emission spectra of **Nap1–3** were all observed to shift towards the near infrared region approaching ~750 nm, but their Φ_{PL}s were found to decrease drastically, which might arise from the much intensified non-radiative internal conversion processes in these compounds due to their much lowered energy gaps.[9] Nevertheless, taking into consideration that **Nap1–3** could emit highly efficient red fluorescence in solvents with medium polarity, they might act as promising red EL materials.

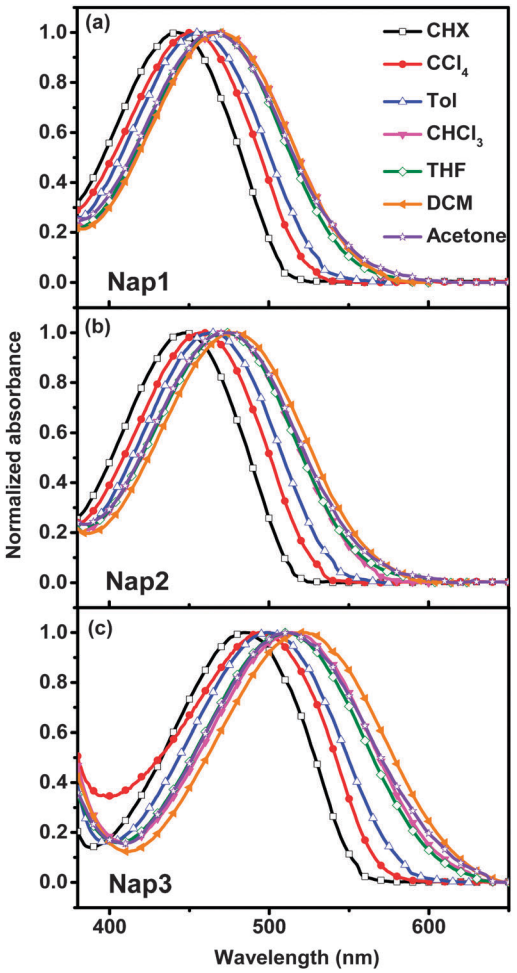

Fig. 2 Normalized absorption spectra of the three objective compounds in solvents with different polarities. (a) **Nap1**; (b) **Nap2**; and (c) **Nap3**.

Table 1 Photophysical data of the three objective molecules in solvents with different polarities (1.0×10^{-5} mol L^{-1})

	NIM[a]			Nap1			Nap2			Nap3		
Solvent	$\lambda_{abs\,max}$ (nm)	$\lambda_{PL\,max}$ (nm)	Φ_{PL}	$\lambda_{abs\,max}$ (nm)	$\lambda_{PL\,max}$ (nm)	Φ_{PL}	$\lambda_{abs\,max}$ (nm)	$\lambda_{PL\,max}$ (nm)	Φ_{PL}	$\lambda_{abs\,max}$ (nm)	$\lambda_{PL\,max}$ (nm)	Φ_{PL}
CHX	—	—	—	440	514	0.22	447	517	0.16	479	553	0.24
CCl_4	—	—	—	450	543	0.29	457	546	0.28	488	567	0.42
Tol	448	552	0.81	461	580	0.42	468	585	0.42	505	622	0.24
$CHCl_3$	461	624	0.36	471	634	0.62	479	637	0.64	511	680	0.45
THF	450	607	0.54	466	655	0.59	473	658	0.54	510	696	0.29
CH_2Cl_2	—	—	—	470	669	0.51	477	672	0.50	519	722	0.09
Acetone	448	658	0.06	464	698	0.08	471	702	0.08	510	750	0.00

[a] Photophysical data derived from ref. 24; $\lambda_{abs\,max}$: absorption maximum; $\lambda_{PL\,max}$: PL emission maximum; Φ_{PL}: absolute PL quantum yield.

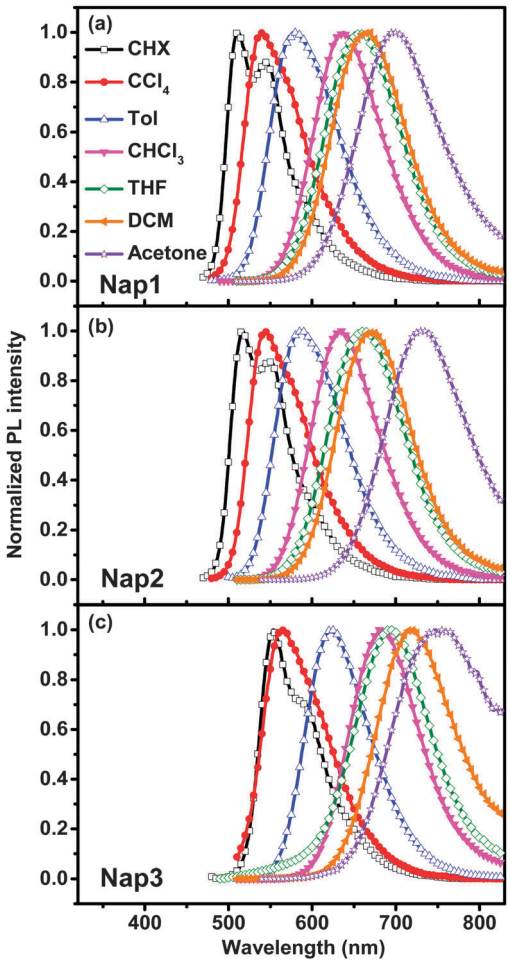

Fig. 3 Normalized PL emission spectra of the three objective compounds in solvents with different polarities. (a) **Nap1**; (b) **Nap2**; and (c) **Nap3**.

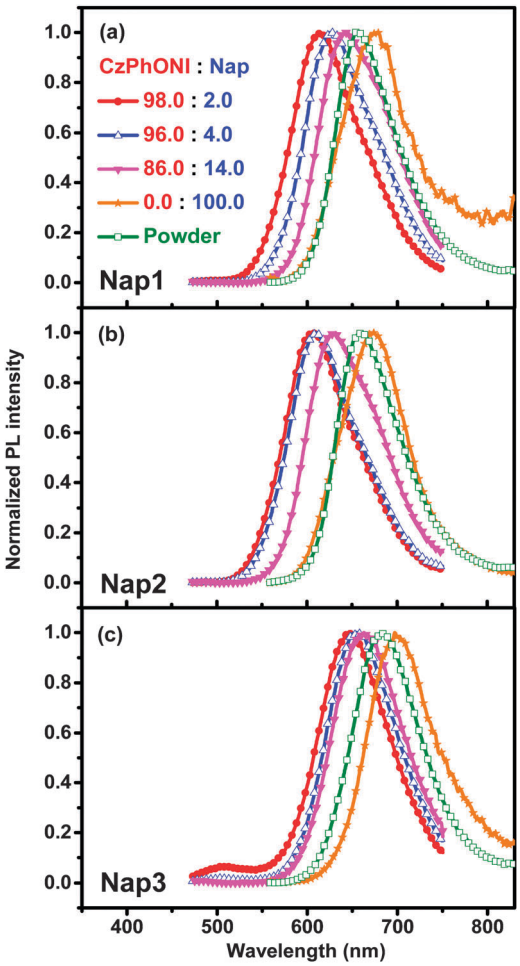

Fig. 4 Normalized PL emission spectra of the **Nap**–**CzPhONI** blend films (λ_{ex} = 390 nm) and the crystalline powder samples as well as the neat film samples of **Nap1–3** (λ_{ex} = 490 nm). (a) **Nap1**; (b) **Nap2**; and (c) **Nap3**.

3.2 PL emission properties in crystalline powder and thin film states

To investigate their potential as red light-emitting materials in OLEDs, PL emission spectra of **Nap1–3** in crystalline powder and thin film states were obtained. As shown in Fig. 4 and Table 2, in both powder and film states, all the three compounds could emit standard-red fluorescence with $\lambda_{PL\,max}$ of 660–700 nm, and **Nap3** shows the most red-shifted emission band. In each case, the PL spectrum of the film sample of **Nap** was slightly broader and red-shifted than that of the crystalline powder sample, which should be attributed to the different molecular conformations in the crystalline and amorphous states.[30]

Despite the fact that in dilute solutions, the fluorescence band of **Nap2** was slightly red-shifted compared to **Nap1**, its $\lambda_{PL\,max}$ was observed to be 6 nm blue-shifted compared to **Nap1** in the neat film state (669 nm *vs.* 675 nm), and its Φ_{PL} was also higher than that of **Nap1** (0.02 *vs.* 0.01). Hence, we could infer

Table 2 Fluorescence data and PLQYs of **Nap**–**CzPhONI** blend films, neat films and crystalline powders of the three objective molecules

	Nap1		**Nap2**		**Nap3**	
Doping ratio (wt%)	$\lambda_{PL\,max}$[a] (nm)	Φ_{PL}[a]	$\lambda_{PL\,max}$[a] (nm)	Φ_{PL}[a]	$\lambda_{PL\,max}$[a] (nm)	Φ_{PL}[a]
2	613	0.37	608	0.46	646	0.23
4	622	0.29	612	0.38	655	0.21
14	641	0.16	632	0.27	663	0.15
Neat film	678	0.01	673	0.02	703	0.01
Powder	659	0.01	659	0.04	680	0.02

[a] λ_{ex} = 390 nm for the blend films; λ_{ex} = 490 nm for the neat films and crystalline powders.

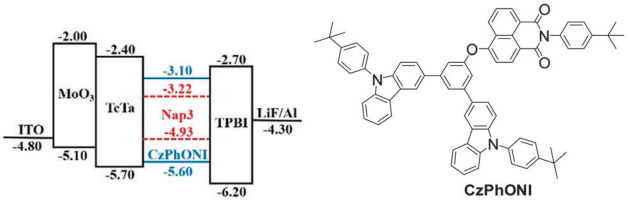

Fig. 5 Device configuration and energy band diagram of devices **I**, **II**, and **III** (left); and molecular structure of the host compound **CzPhONI** (right).

that the presence of the more bulky 2,6-di(isopropyl)phenyl rather than a *n*-hexyl group in **Nap2** should be propitious to the suppression of intermolecular interactions of these fluorophores, and hence could promote less concentration quenching. Although the Φ_{PL}s of these neat film samples were rather low ($\leq$0.02), which would limit their potential as high-performance non-doped red EL luminogens, the relatively high Φ_{PL}s of **Nap1–3** in medium-polarity solvents spurred us to prepare guest–host composite films using **Nap1–3** as dopants. As the compound **CzPhONI** (structure shown in Fig. 5) we have developed recently is a high performance host material for an orange naphthalimide guest compound;[23] herein, we chose it as the host material to fabricate **Nap–CzPhONI** guest–host composite films with different doping-levels.

As shown in Fig. 4 and Table 2, for all the three compounds, with increasing concentration of **Nap** from 2 wt% to 14 wt%, the $\lambda_{PL\,max}$ of the corresponding **Nap–CzPhONI** composite film red-shifted gradually. Excitingly, at a relatively high doping-level of 14 wt%, the film samples with **Nap1** and **Nap2** as guests could emit red fluorescence with $\lambda_{PL\,max}$ of 630–640 nm and the 14 wt% **Nap3** composite film could emit standard-red fluorescence with satisfactory chromaticity ($\lambda_{PL\,max}$ = 663 nm). Analogous to the PL emission property of their neat films, in every doping-level, the $\lambda_{PL\,max}$ of **Nap2** was observed to be blue-shifted for 5–10 nm than that of **Nap1**, validating the more suppressed intermolecular interactions in **Nap2** than **Nap1**. In composite films with **Nap1** and **Nap2** as guests, no emission from the **CzPhONI** host ($\lambda_{PL\,max}$ ~500 nm)[23] could be discerned at each doping-level, indicative of the efficient energy transfer between the host and guest compounds. While for **CzPhONI**/**Nap3** composite films, the emission band from **CzPhONI** was discernible at a relatively low doping-level of 2 wt%; hence, the energy transfer efficiency between **CzPhONI** and **Nap3** should not have been as high as that between **CzPhONI** and **Nap1**/**Nap2**.

In comparison with those of the neat films, the Φ_{PL}s of the guest–host blend film samples were much improved (Table 2). For all the three compounds, the highest PLQYs of the blend films were obtained at the lowest doping-level of 2 wt%. With increasing guest doping ratios from 2 wt% to 14 wt%, the Φ_{PL} of **Nap1**-based film dropped considerably from 0.37 to 0.16, while the Φ_{PL}s of **Nap2**- and **Nap3**-based samples were lowered from 0.46 to 0.27 and from 0.23 to 0.15, respectively, both were less significant than that of the **Nap1**-based one, indicating that **Nap2** and **Nap3** showed more alleviated self-quenching relative to **Nap1**. Consequently, owing to the concurrent presence of a strong electron-donating TMJ group and a bulky 2,6-di(isopropyl)-phenyl substituent, **Nap3** possesses not only an extended π-conjugation system, but also alleviated concentration quenching; hence, it is a perspective candidate as a standard-red EL material.

3.3 Electrochemical properties

To estimate the energy levels of the frontier orbitals of **Nap1–3**, their electrochemical properties were investigated by cyclic voltammetry (CV) in degassed 5 × 10^{-4} mol L^{-1} anhydrous acetonitrile solutions with the Fc/Fc^{+} redox couple as the external standard, and the cyclic voltammograms are shown in Fig. S2 (in ESI†). During the anodic scan from 0 V to 0.50 V, both **Nap1** and **Nap2** showed reversible oxidation waves with half wave potentials ($E_{1/2}$) of 0.24 V *vs.* Fc/Fc^{+}, but **Nap3** showed a reversible oxidation wave with $E_{1/2}$ of 0.05 V *vs.* Fc/Fc^{+}. Upon cathodic scanning from 0 V to −1.95 V, **Nap1** showed a reversible reduction wave with $E_{1/2}$ of −1.70 V *vs.* Fc/Fc^{+}, while both **Nap2** and **Nap3** showed reversible reduction waves with $E_{1/2}$ of −1.66 V *vs.* Fc/Fc^{+}. Hence, the calculated electrochemical band-gaps of **Nap1–3** were 1.94 eV, 1.90 eV and 1.71 eV in sequence, which were consistent with their optical bandgaps (2.19 eV, 2.17 eV and 1.85 eV for **Nap1–3** in sequence) deduced from the onset of their UV-Vis absorption spectra in dilute acetonitrile solutions (Fig. S3 in ESI†).

In comparison with the Fc/Fc^{+} redox couple whose energy level is −4.88 eV in vacuum,[31] the HOMO energy levels of **Nap1–3** were calculated to be −5.12 eV, −5.12 eV and −4.93 eV, and their LUMO energy levels are calculated to be −3.18 eV, −3.22 eV and −3.22 eV, respectively. As the HOMO and LUMO energy levels of **CzPhONI** are −5.60 eV and −3.10 eV, respectively,[23] the HOMO energy difference between **CzPhONI** and **Nap1–3** was 0.48 eV, but that between the HOMOs of **CzPhONI** and **Nap3** was as large as 0.67 eV. Hence, **CzPhONI** should be a more ideal host material for **Nap1–2** than **Nap3**, which may account for the more efficient energy transfer process between **CzPhONI** and **Nap1–2** than **Nap3**.

3.4 Electroluminescent properties

Based on these photophysical and electrochemical experimental results, thermo-evaporated OLEDs with a **Nap3**–**CzPhONI** composite film as light-emitting layer (EML) were fabricated. The device structure was ITO/MoO_3 (1 nm)/TcTa (40 nm)/**CzPhONI**:**Nap3** (*x* wt%) (20 nm)/TPBI (45 nm)/LiF (1 nm)/Al (80 nm), wherein TcTa (4,4′,4″-tri(*N*-carbazolyl)triphenylamine) served as

the hole-transporting material (HTM) and TPBI (1,3,5-tris(1-phenyl-1*H*-benzo[*d*]imidazol-2-yl)benzene) served as the electron-transporting material (ETM). The energy level diagram of the devices is shown in Fig. 5. According to the PL characterization results, device **I**, **II** and **III** with **Nap3** concentrations of 2 wt%, 4 wt% and 14 wt%, respectively, were prepared. The EL spectra and the luminance–voltage–current density (*L*–*V*–*J*) characteristics of devices **I**–**III** are shown in Fig. 6, and some representative EL performance data are summarized in Table 3.

Devices **I**–**III** all displayed bias-independent EL spectra with $\lambda_{EL\,max}$ of 636 nm, 644 nm and 657 nm (vide Fig. 6a and Fig. S4 in ESI†), and CIE coordinates of (0.62,0.37), (0.65,0.34) and (0.67,0.32), respectively. Hence, devices **I** and **II** can emit red EL, but device **III** shows standard-red EL with satisfactory chromaticity. Compared with the corresponding PL spectra of their EML, the EL spectra of all the devices are much broadened and slightly blue-shifted. Because the emission band of **Nap3** correlated highly with the environmental polarity and the EML of the OLEDs was as thin as 20 nm, carrier recombination may have occurred not only within the EML, but also at the TcTa/EML or EML/TPBI interfaces; this may account for the broadened and blue-shifted EL spectra of these devices. In addition, although the emission from **CzPhONI** is discernible in the PL spectrum of the 2 wt% **Nap3**–**CzPhONI** composite film, it could not be observed in the EL spectrum of device **I**, indicative of the more efficient energy transfer and/or charge carrier trapping on **Nap3** in the EL process. As shown in Fig. 6b, under similar driving voltages, the current density of device **II** was lower than that of device **I**, but that of the more heavily doped device **III** is comparable with that of device **I**. Consequently, it should be the energy transfer mechanism that dominates the EL emission process in device **I** and **II** whose guest doping-levels are relatively low, but it should be the direct charge carrier trapping mechanism that governs the EL process in device **III**.[32] In fact, according to the energy level diagram of the devices (Fig. 5), **Nap3** should act as efficient hole-carrier traps due to its much higher HOMO energy level than that of the host and HTM.

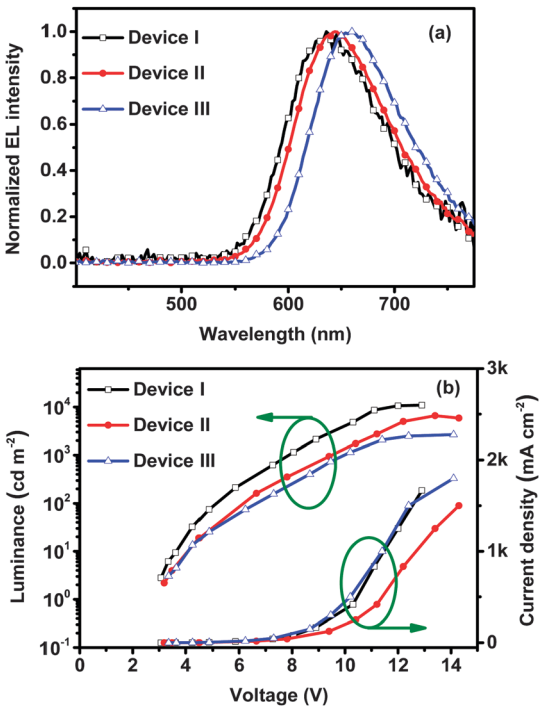

Fig. 6 (a) EL spectra of the three devices (under driving current density of 0.5 mA cm^{-1}); (b) luminance–voltage–current density characteristics of the devices.

Table 3 EL characteristics of the devices using **Nap3** as the guest dopant

Device	V_{on} (V)	L_{max} (cd m^{-2})	EQE$_{max}$ (%)	CE$_{max}$ (cd A^{-1})	$\lambda_{EL\,max}$ (nm)	CIE (*x*,*y*)
I	3.1	10 900	2.1	1.9	636	(0.62,0.37)
II	3.1	6600	1.8	1.1	644	(0.65,0.34)
III	3.1	2660	1.8	0.7	657	(0.67,0.32)

All the three devices display comparable turn-on voltages of 3.1 V. Device **I** exhibits relatively high EL performance with L_{max}, CE$_{max}$ and EQE$_{max}$ of 10 900 cd m^{-2}, 1.9 cd A^{-1} and 2.1%, respectively, indicating that **Nap3** is a quite promising guest compound for OLED applications. However, the chromaticity of this device was still unsatisfactory. With increasing doping-level to 4 wt%, the resulting device **II** showed EL that approaches a standard-red emission with L_{max}, CE$_{max}$ and EQE$_{max}$ values of 6600 cd m^{-2}, 1.1 cd A^{-1} and 1.8%, respectively. For device **III** with a further increased doping-level, it could emit standard-red EL with a L_{max} of 2660 cd m^{-2}, CE$_{max}$ of 0.7 cd A^{-1}, and EQE$_{max}$ of 1.8%. It should be pointed out that compared with the state-of-art standard-red electrofluorescent OLEDs, the PLQYs of the active layers using **Nap3** as a guest dopant were unsatisfactory, which may eventually limit the efficiency of the devices. Nevertheless, as the dilute chloroform solution of **Nap3** could emit standard-red fluorescence with a Φ_{PL} value of ~0.45, the PLQY of the EML with **Nap3** as the guest compound might be enhanced drastically if more appreciate host material were used. Moreover, the device structure, doping level and layer thickness used here have not been optimized for either low driving voltage or high efficiency, thus much improved EL performance should be expected after further optimization has been carried out to resolve these issues.

4. Conclusions

Using electron-rich arylamino groups as the donor constructive units, three red-emissive naphthalimide derivatives were designed and synthesized, and correlations between the molecular structures and photophysical properties of these compounds have been investigated. The results indicated that the presence of a more electron-donating 1,1,7,7-tetramethyljulolidin-9-yl in these fluorophores would endow them with more red-shifted emission bands, while the presence of a bulky 2,6-di(isopropyl)phenyl group on the imide nitrogen atom of these luminogens would reduce their intermolecular interactions. Consequently, the objective compound **Nap3** bearing both 1,1,7,7-tetramethyljulolidin-9-yl and 2,6-di(isopropyl)phenyl groups not only showed standard-red

fluorescence with satisfactory chromaticity, but it also showed suppressed concentration quenching behaviour. Using **Nap3** as the guest dopant, a heavily doped standard-red OLED was achieved with CIE coordinates, EQE_{max} and CE_{max} values of (0.67,0.32), 1.8% and 0.7 cd A^{-1}, respectively. To the best of our knowledge, this is the first example of a standard-red-emissive 1,8-naphthalimide derivative for OLED applications. All these preliminary results indicated that through rational molecular design, 1,8-naphthalimide derivatives could act as quite promising standard-red light-emitting materials for OLED applications.

Acknowledgements

We acknowledge the financial support for this study by the National Natural Science Foundation of China (Project No. 21372168, 21190031 and 21321061) and the CAS Innovation Program. We are also grateful to the Comprehensive Training Platform of Specialized Laboratory, College of Chemistry, SCU and the Analytical and Testing Center, SCU for providing NMR, FT-IR and HRMS data of the intermediates and objective compounds.

Notes and references

1 For reviews, see: (*a*) C. Fan and C. Yang, *Chem. Soc. Rev.*, 2014, **43**, 6439–6469; (*b*) L. Bao and M. D. Heagy, *Curr. Org. Chem.*, 2014, **18**, 740–772; (*c*) M. Zhu and C. Yang, *Chem. Soc. Rev.*, 2013, **42**, 4963–4976; (*d*) C. Murawski, K. Leo and M. C. Gather, *Adv. Mater.*, 2013, **25**, 6801–6827; (*e*) S. Schmidbauer, A. Hohenleutner and B. König, *Adv. Mater.*, 2013, **25**, 2114–2129; (*f*) H. Sasabe and J. Kido, *J. Mater. Chem. C*, 2013, **1**, 1699–1707; (*g*) Y. Chen and D. Ma, *J. Mater. Chem.*, 2012, **22**, 18718–18734.

2 (*a*) A. Benor, S.-Y. Takizawa, C. Pérez-Bolívar and P. Anzenbacher, *Org. Electron.*, 2010, **11**, 938–945; (*b*) J.-H. Jou, J.-R. Tseng, K.-Y. Tseng, W.-B. Wang, Y.-C. Jou, S.-M. Shen, Y.-L. Chen, W.-Y. Huang, S.-Z. Chen, T.-Y. Ding and H.-C. Wang, *Org. Electron.*, 2012, **13**, 2893–2897.

3 (*a*) T. Peng, G. Li, Y. Liu, Y. Wu, K. Ye, D. Yao, Y. Yuan, Z. Hou and Y. Wang, *Org. Electron.*, 2011, **12**, 1068–1072; (*b*) J. W. Sun, J.-H. Lee, C.-K. Moon, K.-H. Kim, H. Shin and J.-J. Kim, *Adv. Mater.*, 2014, **26**, 5684–5688.

4 J. Chen and D. Ma, *J. Lumin.*, 2007, **122–123**, 636–638.

5 T. Arakane, M. Funahashi, H. Kuma, K. Fukuoka, K. Ikeda, H. Yamamoto, F. Moriwaki and C. Hosokawa, *SID Digest*, 2006, **37**, 37–40.

6 (*a*) B.-J. Jung, J.-I. Lee, H. Y. Chu, L.-M. Do, J. Lee and H.-K. Shim, *J. Mater. Chem.*, 2005, **15**, 2470–2475; (*b*) Y. Qiu, P. Wei, D. Zhang, J. Qiao, L. Duan, Y. Li, Y. Gao and L. Wang, *Adv. Mater.*, 2006, **18**, 1607–1611; (*c*) Z. Zhao, J. Geng, Z. Chang, S. Chen, C. Deng, T. Jiang, W. Qin, J. W. Y. Lam, H. S. Kwok, H. Qiu, B. Liu and B. Z. Tang, *J. Mater. Chem.*, 2012, **22**, 11018–11021; (*d*) K. H. Lee, Y. K. Kim and S. S. Yoon, *J. Nanosci. Nanotechnol.*, 2012, **12**, 4203–4206; (*e*) W. Li, Y. Pan, R. Xiao, Q. Peng, S. Zhang, D. Ma, F. Li, F. Shen, Y. Wang, B. Yang and Y. Ma, *Adv. Funct. Mater.*, 2014, **24**, 1609–1614; (*f*) W. Zhang, Z. He, Y. Wang and S. Zhao, *Thin Solid Films*, 2014, **562**, 299–306.

7 S. Forget, S. Chenais, D. Tondelier, B. Geffroy, I. Gozhyk, M. Lebental and E. Ishow, *J. Appl. Phys.*, 2010, **108**, 064509.

8 Y.-T. Lee, C.-L. Chiang and C.-T. Chen, *Chem. Commun.*, 2008, 217–219.

9 X. H. Zhang, B. J. Chen, X. Q. Lin, O. Y. Wong, C. S. Lee, H. L. Kwong, S. T. Lee and S. K. Wu, *Chem. Mater.*, 2001, **13**, 1565–1569.

10 C.-T. Chen, *Chem. Mater.*, 2004, **16**, 4389–4400.

11 (*a*) B.-B. Jang, S. H. Lee and Z. H. Kafafi, *Chem. Mater.*, 2006, **18**, 449–457; (*b*) X. H. Zhang, Z. Y. Xie, F. P. Wu, L. L. Zhou, O. Y. Wong, C. S. Lee, H. L. Kwong, S. T. Lee and S. K. Wu, *Chem. Phys. Lett.*, 2003, **382**, 561–566; (*c*) C. A. Barker, X. Zeng, S. Bettington, A. S. Batsanov, M. R. Bryce and A. Beeby, *Chem. – Eur. J.*, 2007, **13**, 6710–6717.

12 (*a*) J. L. Sessler, V. L. Capuano and A. Harriman, *J. Am. Chem. Soc.*, 1993, **115**, 4618–4628; (*b*) P. D. Rao, S. Dhanalekshmi, B. J. Littler and J. S. Lindsey, *J. Org. Chem.*, 2000, **65**, 7323–7344.

13 (*a*) X. Sun, Y. Liu, X. Xu, C. Yang, G. Yu, S. Chen, Z. Zhao, W. Qiu, Y. Li and D. Zhu, *J. Phys. Chem. B*, 2005, **109**, 10786–10792; (*b*) Y. Li, G. Zhang, G. Yang, Y. Guo, C. Di, X. Chen, Z. Liu, H. Liu, Z. Xu, W. Xu, H. Fu and D. Zhang, *J. Org. Chem.*, 2013, **78**, 2926–2934; (*c*) J.-Y. Yoon, J. S. Lee, S. S. Yoon and Y. W. Kim, *Bull. Korean Chem. Soc.*, 2014, **35**, 1670–1674.

14 (*a*) W.-C. Wu, H.-C. Yeh, L.-H. Chan and C.-T. Chen, *Adv. Mater.*, 2002, **14**, 1072–1075; (*b*) Y.-S. Lee, Z. Lin, Y.-Y. Chen, C.-Y. Liu and T. J. Chow, *Org. Electron.*, 2010, **11**, 604–612.

15 (*a*) X. Sun, X. Xu, W. Qiu, G. Yu, H. Zhang, X. Gao, S. Chen, Y. Song and Y. Liu, *J. Mater. Chem.*, 2008, **18**, 2709–2715; (*b*) B. R. Lee, W. Lee, T. L. Nguyen, J. S. Park, J.-S. Kim, J. Y. Kim, H. Y. Woo and M. H. Song, *ACS Appl. Mater. Interfaces*, 2013, **5**, 5690–5695; (*c*) T. Khanasa, N. Prachumrak, R. Rattanawan, S. Jungsuttiwong, T. Keawin, T. Sudyoadsuk, T. Tuntulani and V. Promarak, *Chem. Commun.*, 2013, **49**, 3401–3403.

16 W. Zhang, Z. He, L. Mu, Y. Zou, Y. Wang and S. Zhao, *Dyes Pigm.*, 2010, **85**, 86–92.

17 (*a*) C. W. Tang, S. A. VanSlyke and C. H. Chen, *J. Appl. Phys.*, 1989, **65**, 3610–3616; (*b*) C. H. Chen, C. W. Tang, J. Shi and K. P. Klubek, *Macromol. Symp.*, 1997, **125**, 49–58; (*c*) B.-J. Jung, C.-B. Yoon, H.-K. Shim, L.-M. Do and T. Zyung, *Adv. Funct. Mater.*, 2001, **11**, 430–434; (*d*) E. J. Na, K. H. Lee, H. Han, Y. K. Kim and S. S. Yoon, *J. Nanosci. Nanotechnol.*, 2013, **13**, 554–557.

18 J. Liu, G. Tu, Q. Zhou, Y. Cheng, Y. Geng, L. Wang, D. Ma, X. Jing and F. Wang, *J. Mater. Chem.*, 2006, **16**, 1431–1438.

19 J. Liu, Y. Wang, G. Lei, J. Peng, Y. Huang, Y. Cao, M. Xie, X. Pu and Z. Lu, *J. Mater. Chem.*, 2009, **19**, 7753–7758.

20 P. Wang, Z. Xie, S. Tong, O. Wong, C.-S. Lee, N. Wong, L. Hung and S. Lee, *Chem. Mater.*, 2003, **15**, 1913–1917.

21 J.-A. Gan, Q. L. Song, X. Y. Hou, K. C. Chen and H. Tian, *J. Photochem. Photobiol., A*, 2004, **162**, 399–406.

22 A. Islam, C.-C. Cheng, S.-H. Chi, S. J. Lee, P. G. Hela, I.-C. Chen and C.-H. Cheng, *J. Phys. Chem. B*, 2005, **109**, 5509–5517.
23 J. Zhou, P. Chen, X. Wang, Y. Wang, Y. Wang, F. Li, M. Yang, Y. Huang, J. Yu and Z. Lu, *Chem. Commun.*, 2014, **50**, 7586–7589.
24 H.-H. Lin, Y.-C. Chan, J.-W. Chen and C.-C. Chang, *J. Mater. Chem.*, 2011, **21**, 3170–3177.
25 C. A. Faler and M. M. Joullié, *Org. Lett.*, 2007, **9**, 1987–1990.
26 (*a*) C.-T. Lee and A. T. Hu, *Dyes Pigm.*, 2003, **59**, 63–69; (*b*) B. Balaganesan, S.-W. Wen and C. H. Chen, *Tetrahedron Lett.*, 2003, **44**, 145–147; (*c*) X. Jiang, X. Yang, C. Zhao, K. Jin and L. Sun, *J. Phys. Chem. C*, 2007, **111**, 9595–9602.
27 F. Yu, Y. Wang, W. Zhu, Y. Huang, M. Yang, H. Ai and Z. Lu, *RSC Adv.*, 2014, **4**, 36849–36853.
28 H. Marom, Y. Popowski, S. Antonov and M. Gozin, *Org. Lett.*, 2011, **13**, 5532–5535.
29 M. Ghasemian, A. Kakanejadifard, F. Azarbani, A. Zabardasti, S. Shirali, Z. Saki and S. Kakanejadifard, *Spectrochim. Acta, Part A*, 2015, **138**, 643–647.
30 C. Y. K. Chan, Z. Zhao, J. W. Y. Lam, J. Liu, S. Chen, P. Lu, F. Mahtab, X. Chen, H. H. Y. Sung, H. S. Kwok, Y. Ma, I. D. Williams, K. S. Wong and B. Z. Tang, *Adv. Funct. Mater.*, 2012, **22**, 378–389.
31 (*a*) X. Liu, B. B. Y. Hsu, Y. Sun, C.-K. Mai, A. J. Heeger and G. C. Bazan, *J. Am. Chem. Soc.*, 2014, **136**, 16144–16147; (*b*) X. Liu, Y. Sun, B. B. Y. Hsu, A. Lorbach, L. Qi, A. J. Heeger and G. C. Bazan, *J. Am. Chem. Soc.*, 2014, **136**, 5697–5708.
32 (*a*) M. A. Wolak, B.-B. Jang, L. C. Palilis and Z. H. Kafafi, *J. Phys. Chem. B*, 2004, **108**, 5492–5499; (*b*) M. A. Wolak, J. Delcamp, C. A. Landis, P. A. Lane, J. Anthony and Z. Kafafi, *Adv. Funct. Mater.*, 2006, **16**, 1943–1949; (*c*) K. H. Lee, M. H. Park, C. S. Kim, Y. K. Kim and S. S. Yoon, *Thin Solid Films*, 2011, **520**, 510–514.